



Article

# An Automatic Algorithm for Mapping Algal Blooms and Aquatic Vegetation Using Sentinel-1 SAR and Sentinel-2 MSI Data

Yihao Xin <sup>1,2</sup>, Juhua Luo <sup>1,2,\*</sup>, Jinlong Zhai <sup>2</sup>, Kang Wang <sup>2</sup>, Ying Xu <sup>2</sup>, Haitao Qin <sup>2</sup>, Chao Chen <sup>3</sup>, Bensheng You <sup>1,\*</sup> and Qing Cao <sup>1</sup>

- State Environmental Protection Key Laboratory of Aquatic Ecosystem Health in the Middle and Lower Reaches of Yangtze River, Nanjing 210036, China; xinyihao21@mails.ucas.ac.cn (Y.X.); caoqing@jshb.gov.cn (Q.C.)
- Key Laboratory of Lake and Watershed Science for Water Security, Nanjing Institute of Geography and Limnology, Chinese Academy of Sciences, Nanjing 211135, China; y22301013@stu.ahu.edu.cn (J.Z.); kangw1803@gmail.com (K.W.); xuying23@mails.ucas.ac.cn (Y.X.); qinhaitao221@mails.ucas.ac.cn (H.Q.)
- <sup>3</sup> School of Geography Science and Geomatics Engineering, Suzhou University of Science and Technology, Suzhou 215009, China; chenchao@usts.edu.cn
- \* Correspondence: jhluo@niglas.ac.cn (J.L.); youbs@jshb.gov.cn (B.Y.)

Abstract: Aquatic vegetation, including floating-leaved and emergent aquatic vegetation (FEAV), submerged aquatic vegetation (SAV), and algal blooms (AB), are primary producers in eutrophic lake ecosystems and hold significant ecological importance. Aquatic vegetation and AB dominate in clear and turbid water states, respectively. Monitoring their dynamics is essential for understanding lake states and transitions. Sentinel imagery provides highresolution data for capturing changes in aquatic vegetation and AB. However, the existing mapping algorithms for aquatic vegetation and AB based on Sentinel data only focused on one or two types. There are still limited algorithms that comprehensively reflect the dynamic changes of aquatic vegetation and AB. Additionally, the unique red-edge bands of Sentinel-2 MSI have not yet been fully exploited for mapping aquatic vegetation and AB. Therefore, we developed an automated mapping algorithm that utilizes Sentinel data, especially red-edge bands, to comprehensively reflect the dynamic changes of FEAV, SAV, and AB. The key indicator of the algorithm, the second principal component (PC2) derived from four red-edge bands and four other bands of Sentinel-2 MSI, can effectively distinguish between FEAV and AB. SAV was mapped by the Sentinel-based submerged aquatic vegetation index (SSAVI), which was constructed by fusing Sentinel-1 SAR and Sentinel-2 MSI data. The algorithm was tested in three representative lakes, including Lake Taihu, Lake Hongze, and Lake Chaohu, and yielded an average accuracy of 87.65%. The algorithm was also applied to track changes in aquatic vegetation and AB from 2019 to 2023. The results show that, over the past five years, AB coverage in all three lakes has decreased. The coverage of aquatic vegetation in Lake Taihu and Lake Hongze is also declining, while coverage remains relatively stable in Lake Chaohu. This algorithm leverages the high spatiotemporal resolution of Sentinel data, as well as its band advantages, and is expected to be applicable for large-scale monitoring of aquatic vegetation and AB dynamics. It will provide valuable technical support for future assessments of lake ecological health and state transitions.

**Keywords:** remote sensing; submerged aquatic vegetation; floating-leaved and emergent aquatic vegetation; algal blooms; sentinel data



Academic Editor: Paul Aplin

Received: 11 January 2025 Revised: 28 February 2025 Accepted: 6 March 2025 Published: 12 March 2025

Citation: Xin, Y.; Luo, J.; Zhai, J.; Wang, K.; Xu, Y.; Qin, H.; Chen, C.; You, B.; Cao, Q. An Automatic Algorithm for Mapping Algal Blooms and Aquatic Vegetation Using Sentinel-1 SAR and Sentinel-2 MSI Data. *Land* 2025, 14, 592. https:// doi.org/10.3390/land14030592

Copyright: © 2025 by the authors. Licensee MDPI, Basel, Switzerland. This article is an open access article distributed under the terms and conditions of the Creative Commons Attribution (CC BY) license (https://creativecommons.org/licenses/by/4.0/).

Land 2025, 14, 592 2 of 18

# 1. Introduction

Aquatic vegetation is typically categorized into emergent and floating-leaved aquatic vegetation (FEAV), which grows above the water, and submerged aquatic vegetation (SAV), which grows underwater. They are the primary producer in lake ecosystems, and performs a crucial ecological role, including carbon sink, regulating nutrient levels and enhancing water clarity [1–3]. These ecological functions of aquatic vegetation are crucial for maintaining the clear state of lakes, and preventing the transition to the turbid state dominated by algal bloom (AB) [4]. However, with the increase in agricultural fertilizer consumption and the rise in global temperatures, the area of algal blooms has reached 11.7% of the global lake area over the past 40 years [5,6]. This has emerged as one of the most severe environmental problems in inland waters, posing grave threats to both public health and aquatic ecosystems worldwide. At the same time, under various stressors such as eutrophication, aquaculture cultivation, and global climate changes, aquatic vegetation, is also experiencing accelerated degradation [5,6]. This phenomenon may imply that lakes are transitioning from the clear state to the turbid state. Therefore, monitoring the dynamics of aquatic vegetation and AB is an urgent need for understanding lake state transitions and evaluating the health of lake ecosystems.

Traditional field surveys for collecting aquatic vegetation and AB data are often timeconsuming and labor-intensive. The limited datasets obtained from these surveys fail to capture the complex spatiotemporal heterogeneity of aquatic vegetation and AB. In contrast, satellite remote sensing has significant advantages, including wide coverage, regular revisit capabilities, and long-term observational data. This makes it an effective solution for addressing lack in regional or global-scale aquatic vegetation and AB in eutrophic lakes. Although the spectral responses of aquatic vegetation and AB are very similar in certain bands [7–9], an numerous algorithm has been developed for mapping aquatic vegetation and AB using optical remote sensing data [9–11]. Among them, some novel indices were proposed for distinguish aquatic vegetation and AB, such as normalized difference water index based on near infrared and shortwave infrared 1 (NDWI 4,5) [8], macroalgae index (MAI) [9], and aquatic vegetation index (AVI) [10]. These indices enhance the spectral differences between aquatic vegetation and AB, especially between FEAV and AB, and utilize specific thresholds to map FEAV, SAV, and AB. However, most of these indices were developed using Landsat data, and their ability to distinguish aquatic vegetation and AB may decline when applied to Sentinel-2 MSI data. This renders the original threshold determination methods unsuitable and resulting in misclassification [12]. Some machine learning or deep learning models developed for specific lakes are difficult to apply to large-scale monitoring [13–16]. In addition, Sentinel-2 MSI data not only offer higher spatiotemporal resolution than Landsat data but also unique red-edge bands (703 nm, 740 nm, 783 nm, and 864 nm). Spectral indices constructed using red-edge bands, such as the normalized difference red edge index (NDREI), have been widely used for mapping aquatic vegetation [15,17]. Existing studies have also demonstrated that red-edge bands can effectively accurately identify algal blooms, such as normalized difference chlorophyll index (NDCI) [18]. However, these indices often focus on only one type within FEAV or AB. Studies focusing on the use of red-edge bands to distinguish aquatic vegetation and AB in eutrophic lakes remain limited. Overall, the advantages of Sentinel-2 MSI data, such as its high spatiotemporal resolution and unique red-edge bands, have not been fully exploited in monitoring aquatic vegetation and AB.

To address these issues, we aim to develop a new automatic algorithm for mapping FEAV, SAV and AB using Sentinel data in eutrophic lakes with coexistence of aquatic vegetation and AB. The specific objectives include: (1) constructing a new band combination based on the unique red edge bands of Sentinel-2 MSI to distinguish FEAV and AB;

Land 2025, 14, 592 3 of 18

(2) developing a comprehensive algorithm for mapping FEAV, SAV, and AB by integrating Sentinel-based submerged aquatic vegetation index (SSAVI); (3) validating the algorithm and obtaining the annual and interannual changes of FEAV, SAV, and AB from 2019 to 2023 in Lake Taihu, Lake Chaohu, and Lake Hongze.

#### 2. Materials

#### 2.1. Study Area

We selected three eutrophic lakes with as study lakes, including Lake Taihu (30°55′–31°32′ N, 119°52′–120°36′ E), Lake Chaohu (31°25′–31°43′ N, 117°17′–117°52′ E), and Lake Hongze (33°06′–33°40′ N, 118°10′–118°51′ E) (Figure 1). These lakes are shallow lakes, and the water depth is less than 3 m. Among them, Lake Taihu is a typical vegetationalgae coexisting lake. The western region of Lake Taihu frequently experiences algal blooms, making it an algae-dominated area, while aquatic vegetation is widely distributed in the eastern part of the lake, especially in the East Bay of Lake Taihu [19,20]. Therefore, Lake Taihu serves as an ideal testing ground for developing classification algorithms for algal blooms and aquatic vegetation. In addition, Lake Chaohu is an algae-dominated lake, with sparse aquatic vegetation distributed only in the littoral zones [21]. Lake Hongze is a vegetation-dominated lake, with occasional algal blooms (Table S1) [14]. These two lakes, with markedly different aquatic environments, can be used to validate the generalizability of the algorithm.

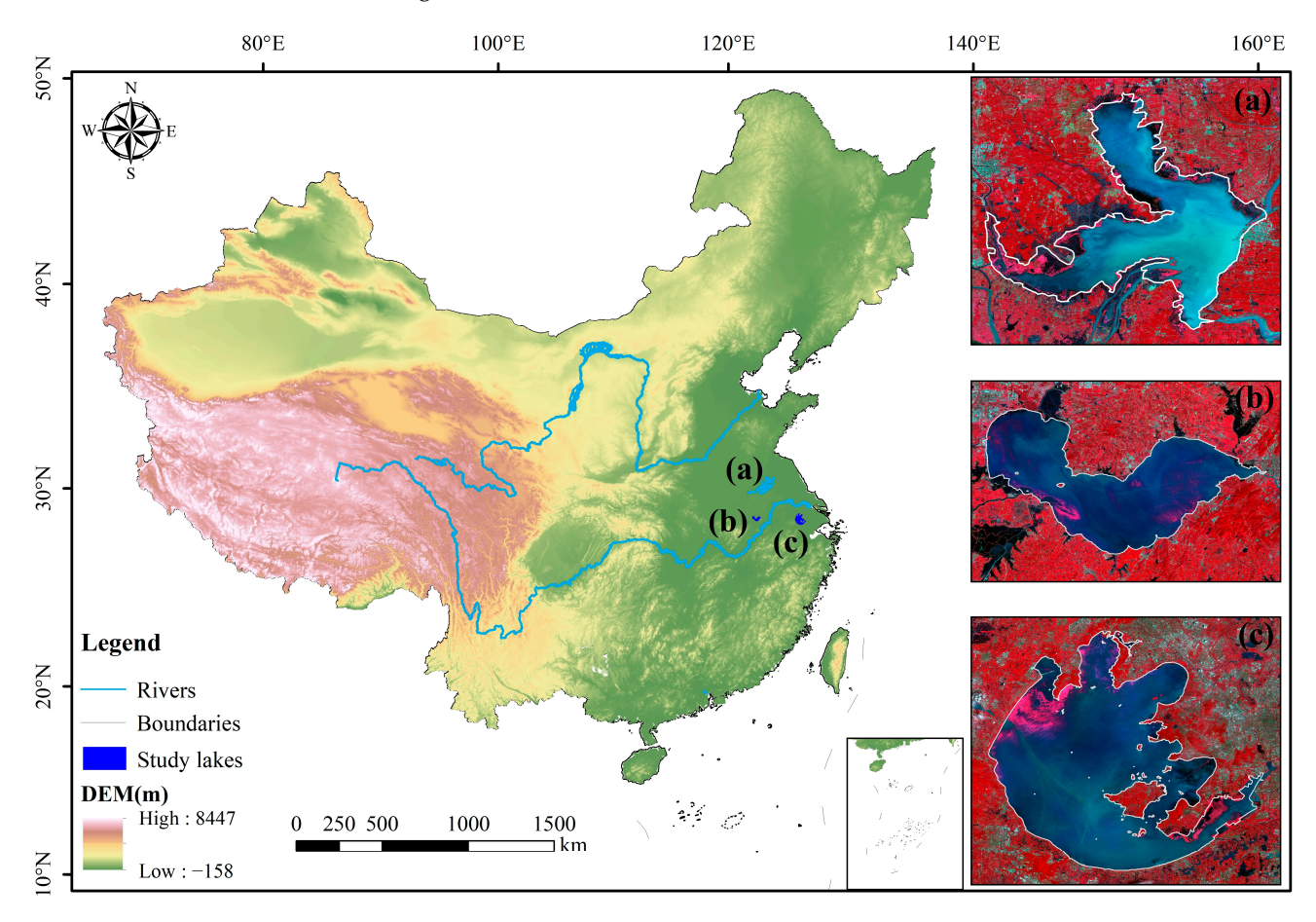


Figure 1. Location of the three study lakes. (a) Lake Hongze, (b) Lake Chaohu, (c) Lake Taihu.

Land 2025, 14, 592 4 of 18

#### 2.2. Satellite Data

We used data from the European Space Agency's Sentinel satellite series in this study, including Sentinel-1 and Sentinel-2. The Sentinel-2 MSI data have 13 spectral bands with a maximum revisit cycle of five days and a resolution of 10 m. The Google Earth Engine (GEE) platform offers Sentinel-2 MSI data products Level-2A, which includes topof-atmosphere (TOA) reflectance data with preprocessing steps encompassing radiometric calibration, geometric correction, and atmospheric correction. The API of the dataset in GEE is "COPERNICUS/S2". To ensure image usability, each image was clipped to the study lake boundaries from the HydroLAKES dataset and cloud masking was applied using the QA60 band. In addition, Sentinel-1 is equipped with a C-band synthetic aperture radar (SAR) operating at a frequency of 5.405 GHz, with a maximum revisit interval of six days. We used Sentinel-1 Interferometric Wide Swath mode, which includes VV and VH polarization bands. The SAR data were processed with ground range detection, orbit correction, terrain correction, and thermal noise reduction to create ground-projected images with a spatial resolution of 10 m. The API of the dataset in GEE is "COPERNICUS/S1\_GRD". In this study, Sentinel-1 SAR and Sentinel-2 MSI images were time-matched, with the SAR images selected closest in date to the Sentinel-2 MSI acquisition [22,23]. After time matching, Lee-Sigma filtering was applied to the Sentinel-1 SAR images to further reduce speckle noise [24]. Finally, images were clipped using lake boundaries from the HydroLAKES dataset [25].

#### 2.3. Field Data

We collected 7362 samples using drones and boats on 17 August 2019, and 5 September 2020, in Lake Taihu; on 15 September 2019, in Lake Chaohu; and on 24 and 25 August 2019, in Lake Hongze (Table 1). Among them, the samples from Lake Taihu were used for developing algorithm, including 1220 SAV samples, 2978 FEAV samples, 2475 AB samples and 689 OW samples. In addition, a total of 1404 SAV samples, 3359 FEAV samples, 2768 AB samples, and 999 OW samples from all three lakes, including Lake Taihu, were used for algorithm validation.

Lake Name	Survey Date	Image Date	SAV Samples	FEAV Samples	AB Samples	OW Samples
Taihu	17 August 2019 5 September 2020	17 August 2019 5 September 2020	624 596	1445 1533	1368 1107	356 333
Chaohu	15 September 2019	19 September 2019	74	100	293	108
Hongze	24 August 2019 25 August 2019	20 August 2019	110	281	/	202
Total	/	/	1404	3359	2768	999

**Table 1.** Basic information of survey and samples for FEAV, AB, and OW.

# 3. Method

We developed the algorithm for mapping FEAV, SAV, and AB using Sentinel-1 SAR and Sentinel-2 MSI data (Figure 2). It included two main steps: (1) construction of the Sentinel-based submerged aquatic vegetation index (SSAVI) by fusion of the Sentinel-1 SAR and Sentinel-2 MSI imagery, and then mapping SAV using X-Means clustering; (2) construction of the second principal component (PC2), masking non-vegetation spectral characteristic area, and mapping FEAV and AB using OTSU algorithm.

Land **2025**, 14, 592 5 of 18

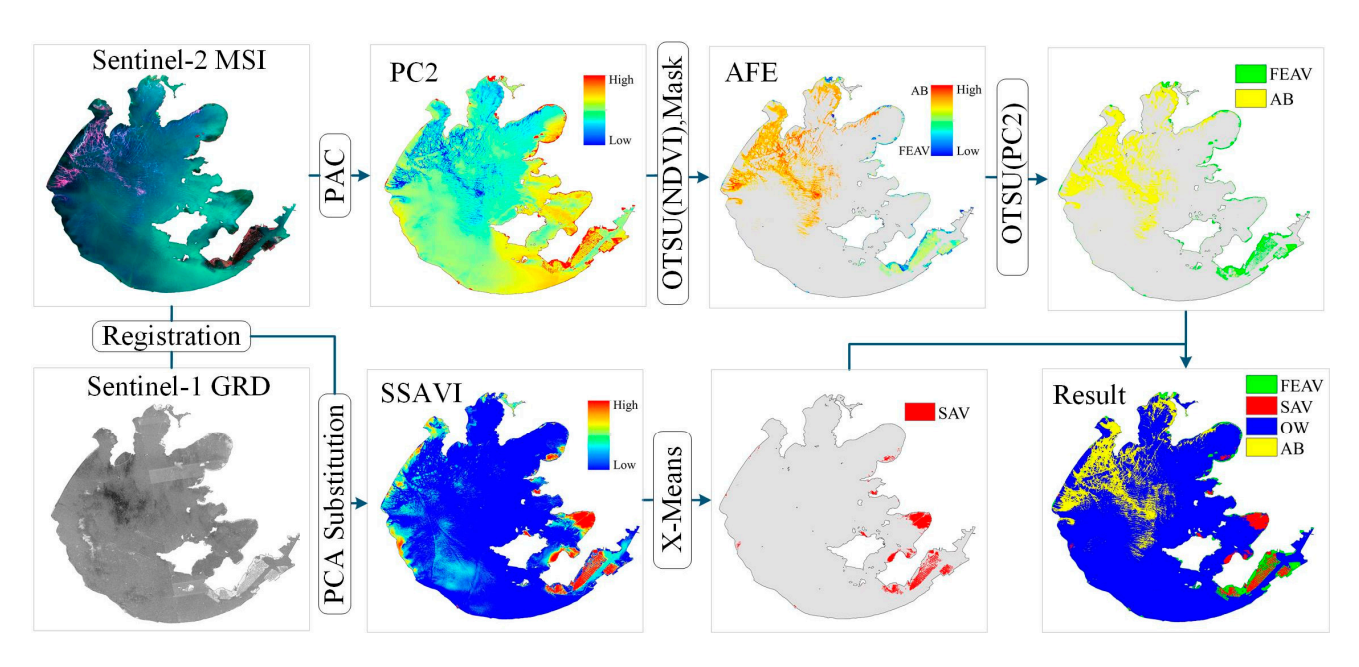


**Figure 2.** Workflow of the algorithm proposed for mapping SAV, FEAV, and AB based on a case in Lake Taihu. In this case, Sentinel-2 MSI TOA and Sentinel-1 GRD images were acquired on 28 July 2018, and 5 August 2018, respectively. Note: AFE represents FEAV and AB.

#### 3.1. Mapping SAV

The Sentinel-based submerged aquatic vegetation index (SSAVI) is an index that is sensitive only to SAV and is not influenced by AB, FEAV and open water (OW) [12]. It was constructed by fusing Sentinel-1 SAR and Sentinel-2 MSI data, and the Principal Component Substitution algorithm [26,27] (Equations (1)–(3)). Specifically, we replaced the first principal component of the six bands (Blue, Green, Red, NIR, SWIR 1, and SWIR 2) from Sentinel-2 MSI data with the dual-polarization Radar Vegetation Index (RVI<sub>dual</sub>) [28] constructed from Sentinel-1 SAR data. After inverse transforming RVI and the remaining five principal components, the first resulting band is SSAVI. In SSAVI, the value of SAV is consistently high, while FEAV, AB, and OW are all low. Therefore, based on this characteristic, SSAVI can use to extract SAV [12].

$$RVI_{dual} = \frac{\sigma_{VH}}{\sigma_{VV} + \sigma_{VH}}$$
 (1)

$$SSAVI = RVI \times X_{11} + [R_{Blue}, R_{Green}, R_{Red}, R_{NIR}, R_{SWIR1}, R_{SWIR2}] \times Y \tag{2}$$

$$Y = \left[X_{ij}\right] \times \left[X_{1j}\right]^{T} \tag{3}$$

where  $\sigma_{VH}$  and  $\sigma_{VV}$  are the backscattering coefficients for VH (Vertical–Horizontal) and VV (Vertical–Vertical) polarizations. Y is the matrix of weight coefficients that make up the components in SSAVI. R is the reflectance and the subscript is spectral band. X is the  $6 \times 6$  matrix of rotation coefficients produced by PCA transformation, with subscripts representing rows and columns, respectively, i = (1, 2, 3, 4, 5, 6), j = (2, 3, 4, 5, 6).

After obtaining SSAVI, we use X-means clustering to map SAV. X-means clustering is an extension of the K-means clustering algorithm [29]. X-means clustering can automatically determine the optimal number of clusters by calculating the Bayesian Information Criterion (BIC) values corresponding to the clustering results for the given minimum and maximum number of clusters. Specifically, in this study, we set the clustering range from 3 to 8 and obtained the clustering result corresponding to the lowest BIC value (Equation (4)). Finally,

Land 2025, 14, 592 6 of 18

based on the optimal clustering results, the class with the highest mean SSAVI is defined as SAV [12].

$$BIC = kln(n) - 2ln(L) \tag{4}$$

where L is the likelihood of the given model data; k is the number of parameters in the model; n is the sample size.

#### 3.2. Mapping FEAV and AB

The key indicator used in this study to separate FEAV from AB is constructed through Principal Component Analysis (PCA). PCA is a simple dimensionality reduction technique that transforms correlated variables into a new set of linear orthogonal (uncorrelated) variables known as principal components [30]. In aquatic vegetation mapping studies, PCA enhances the independence of spectral data, reduces spectral redundancy, and constructs potential usable indices [31–33]. In this study, we obtained the principal components by performing eigenvalue decomposition on the covariance matrix of the eight normalized bands from Sentinel-2 MSI imagery, including the green band (B3), red edge bands (B5-7, B8A), near-infrared band (B8), and short-wave infrared bands (B11, B12) (Decomposition-Factory.eig() from https://ejml.org, accessed on 19 September 2024). Among them, the second principal component (PC2) demonstrated a very significant separation for FEAV and AB (Equation (5)) compared to the other principal components (Figure S1). In PC2, the value of AB is consistently high, while FEAV is low (Figure 3b). Therefore, PC2 can be used for distinguishing FEAV and AB.

$$PC2 = [R_{Green}, R_{RE1}, R_{RE2}, R_{RE3}, R_{NIR}, R_{RE4}, R_{SWIR1}, R_{SWIR2}] \times Y$$
 (5)

where Y is the weight coefficients matrix of principal component analysis. R is the reflectance, and the subscript is spectral band.

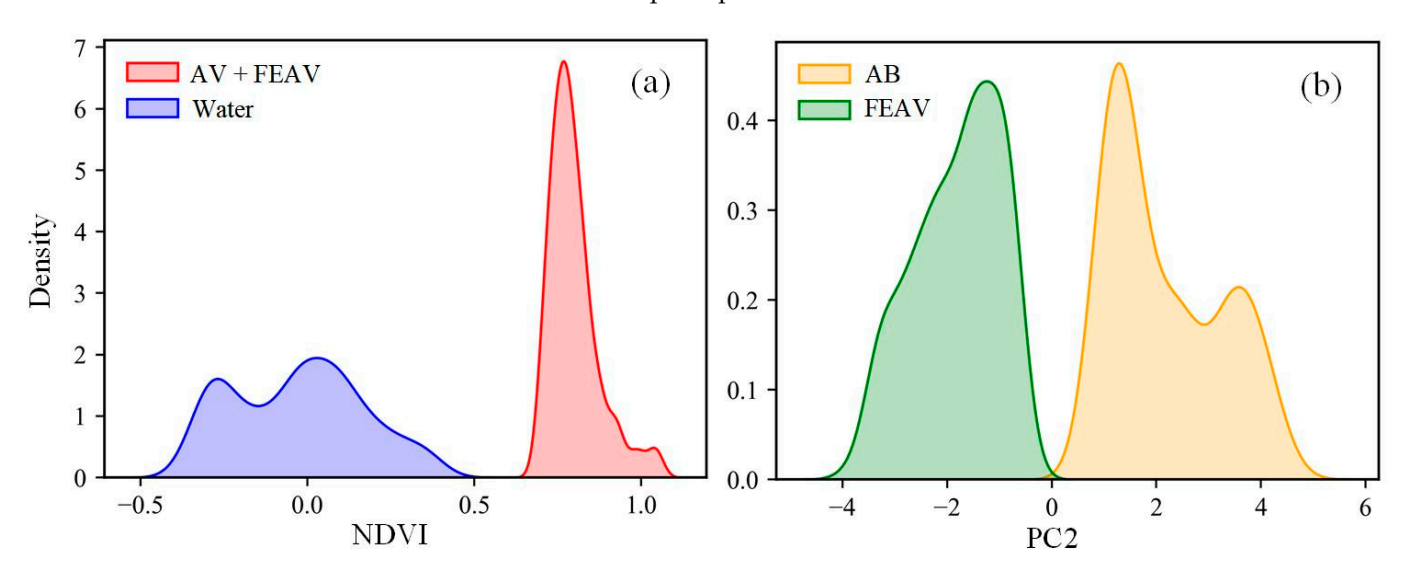


**Figure 3.** Separability of NDVI and PC2 for lake cover types. (a) Separability for water, and AV and FEAV in NDVI. (b) Separability for AB and FEAV in PC2.

In addition, we also used NDVI to eliminate interference from other lake cover types. AB and FEAV exhibit typical vegetation spectral characteristics, showing strong absorption and lower reflectance in the red wavelength range, while demonstrating higher reflectance in the near-infrared wavelength range. NDVI has been shown to effectively identify areas within lakes that exhibit spectral characteristics of vegetation [17,34] (Figure 3a) (Equation (6)).

Land 2025, 14, 592 7 of 18

Therefore, we obtained these regions though NDVI and the threshold of NDVI derived from OTSU algorithm [35] (Equation (7)).

$$NDVI = \frac{R_{Red} - R_{NIR}}{R_{Red} + R_{NIR}}$$
 (6)

$$T = \operatorname{argmax} \left( p_0 \times p_1 \times \left( q_0 - q_1 \right)^2 \right) \tag{7}$$

where  $R_{Red}$  represents the reflectance in the red wavelength band, and  $R_{NIR}$  represents the reflectance in the near-infrared band.  $p_0$  denotes the proportion of foreground pixels in the image;  $p_1$  denotes the proportion of background pixels;  $q_0$  represents the mean value of the foreground;  $q_1$  represents the mean value of the background; and T represents the threshold corresponding to the maximum inter-class variance.

Finally, we also applied the OTSU algorithm to the PC2 of the FEAV and AB regions. The class above the threshold is defined as AB, while the class below the threshold is defined as FEAV.

## 3.3. Assessment of Algorithm

The accuracy and robustness of algorithm proposed in this study are evaluated through two methods:

- (1) Accuracy assessment based on field measured data. Confusion matrices were obtained between measured classes from field measured data and mapped classes derived from the algorithm proposed in this study, and overall accuracy (OA), Kappa, user accuracy (UA) and producer accuracy (PA) were calculated [36].
- (2) Assessment by phenological features of aquatic vegetation. For lakes lacking FEAV and SAV samples, indirect validation was conducted by phenological feature of FEAV and SAV. Specifically, in a short timeframe, FEAV and SAV exhibit fixed spatial distribution and limited area change [37]. The similarity in spatial distribution of FEAV and SAV between adjacent temporally sequential images was assessed by Dice Coefficient [38] (Equation (8)).

$$D = \frac{(2 \times N_x)}{N} \times 100\% \tag{8}$$

where  $N_x$  is the count of pixels concurrently classified as SAV in two images; N is the combined count of pixels classified as SAV in two images; D is Dice Coefficient.

## 4. Result

4.1. Validations of Algorithm

#### 4.1.1. Validations by Field Measured Data

In the three study lakes, the FEAV, SAV, and AB maps were obtained by the algorithm proposed in this study based on Sentinel data, respectively (Figure 4). We validated the algorithm based on field measured data. The OAs were 89.44% and 91.72% in Lake Taihu, 82.61% in Lake Chaohu, 86.84% in Lake Hongze (Table 2). The water environments of the three lakes vary significantly, the algorithm was still able to accurately identify FEAV, SAV, and AB. This demonstrates the algorithm's generalizability.

**Table 2.** Confusion matrix between measured class and mapped class derived from the algorithm in Lake Taihu, Lake Chaohu and Lake Hongze. OA = Overall Accuracy, UA = User Accuracy, PA = Producer Accuracy.

Lake Name/ Image Date					Measure	d Class				
			SAV	FEAV	AB	OW	Sum	UA (%)		
Taihu 17 August 2019	Map class _	SAV	208	4	12	9	233	89.27		
		FEAV	11	454	29	0	494	91.9		
		AB	21	27	406	17	471	86.19		
		OW	14	0	21	330	365	90.41		
		Sum	254	485	468	356	1563			
		PA (%)	81.89	93.61	86.75	92.7				
	OA = 89.44%; Kappa = 0.86									
T. 11			SAV	FEAV	AB	OW	Sum	UA (%)		
		SAV	319	7	13	2	341	93.55		
	Map class _	FEAV	8	489	17	0	514	95.13		
Taihu 5 September		AB	9	22	329	19	379	86.81		
2020		OW	11	0	23	312	346	90.17		
		Sum	347	518	382	333	1580			
		PA (%)	91.92	94.4	86.13	93.69				
			OA	= 91.72%; Ka	appa = 0.89					
Chaohu 19 September 2019			SAV	FEAV	AB	OW	Sum	UA (%)		
	Map class _	SAV	71	2	1	0	74	95.95		
		FEAV	0	90	0	0	90	100		
		AB	3	8	279	16	306	91.18		
		OW	0	0	13	92	105	87.62		
		Sum	74	100	293	108	575			
		PA (%)	95.95	90	95.22	85.19				
	OA = 82.61%; Kappa = 0.73									
Hongze 20 August 2019			SAV	FEAV	AB	OW	Sum	UA (%)		
	Map class _	SAV	103	6	\	2	111	92.79		
		FEAV	1	272	\	0	273	99.63		
		AB	\	\	\	\	\	\		
		OW	6	3	\	200	209	95.69		
	_	Sum	110	281	\	202	593			
		PA (%)	93.64	96.8	\	99.01				
			OA	= 86.84%; Ka	appa = $0.79$					

Land **2025**, 14, 592 9 of 18

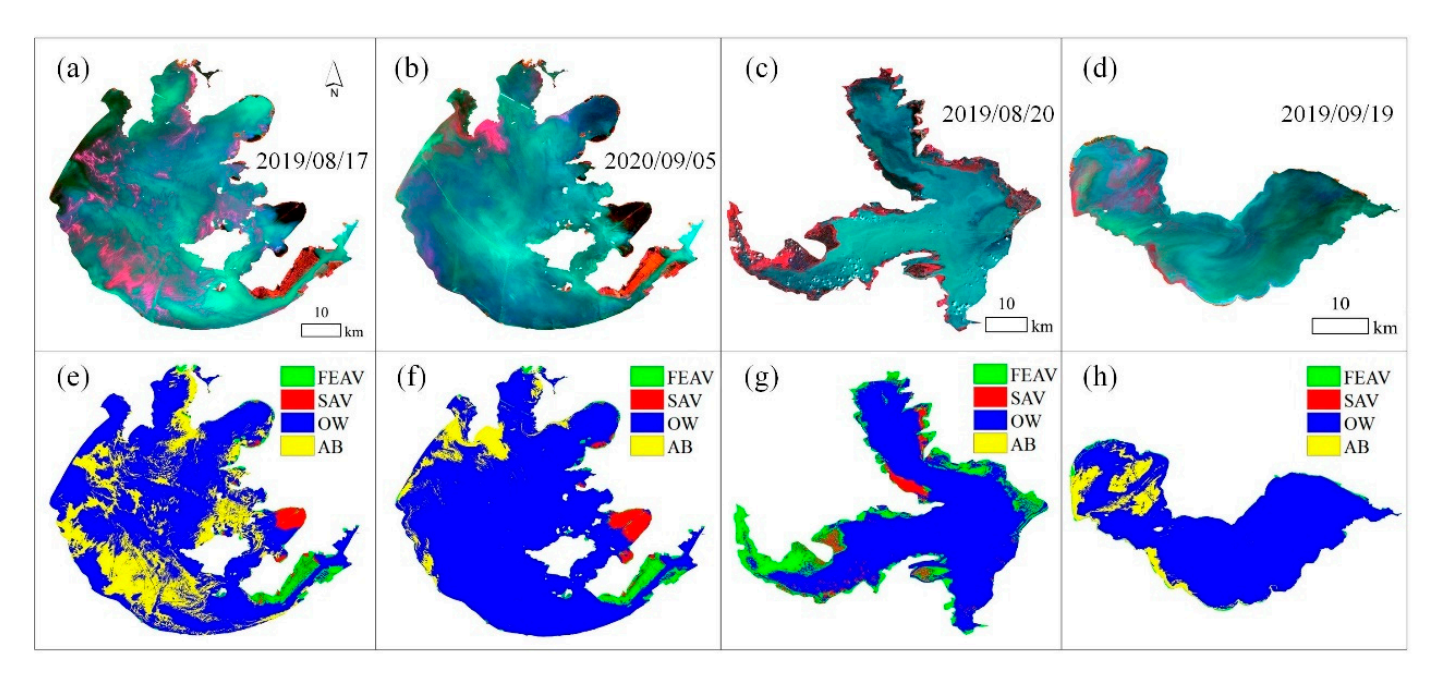


**Figure 4.** (a–d) False color images (NIR, Red, Green) and (e–h) corresponding classification maps derived from our algorithm in Lake Taihu, Lake Hongze, and Lake Chaohu.

# 4.1.2. Assessment by Phenological Feature

The algorithm proposed in this study was applied to imagery of Lake Hongze on 20 August and 30 August 2019, imagery of Lake Chaohu on 19 September and 29 September 2019, as well as imagery of Lake Taihu on 31 October and 5 November 2019 (Figure 5). The results indicated that the spatial distribution and area of SAV and FEAV demonstrated a high level of overall consistency. Specifically, in Lake Hongze, with a ten-day interval between images, the SAV areas were 84.8 km² and 81.3 km², and the FEAV areas were 320.7 km² and 297.5 km², with the Dice Coefficient of 79.01% (Figure 5a,b). In Lake Chaohu, with a ten-day interval between images, the FEAV was sparsely distributed along the western coastal zone, and the areas were 10.6 km² and 10.5 km², respectively (Figure 5a,b). In Lake Taihu, the two images were taken nearly 5 days apart (Figure 5c,d). SAV was primarily distributed in East Lake Taihu and Xukou Bay, covering areas of 86.5 km² and 103.5 km², and FEAV was mainly distributed in East Lake Taihu Bay, with areas of 97.3 km² and 85.8 km² (Figure 5e,f). There are still slight differences observed in maps of different periods, and this may mainly be due to the growth and death of SAV and FEAV itself.

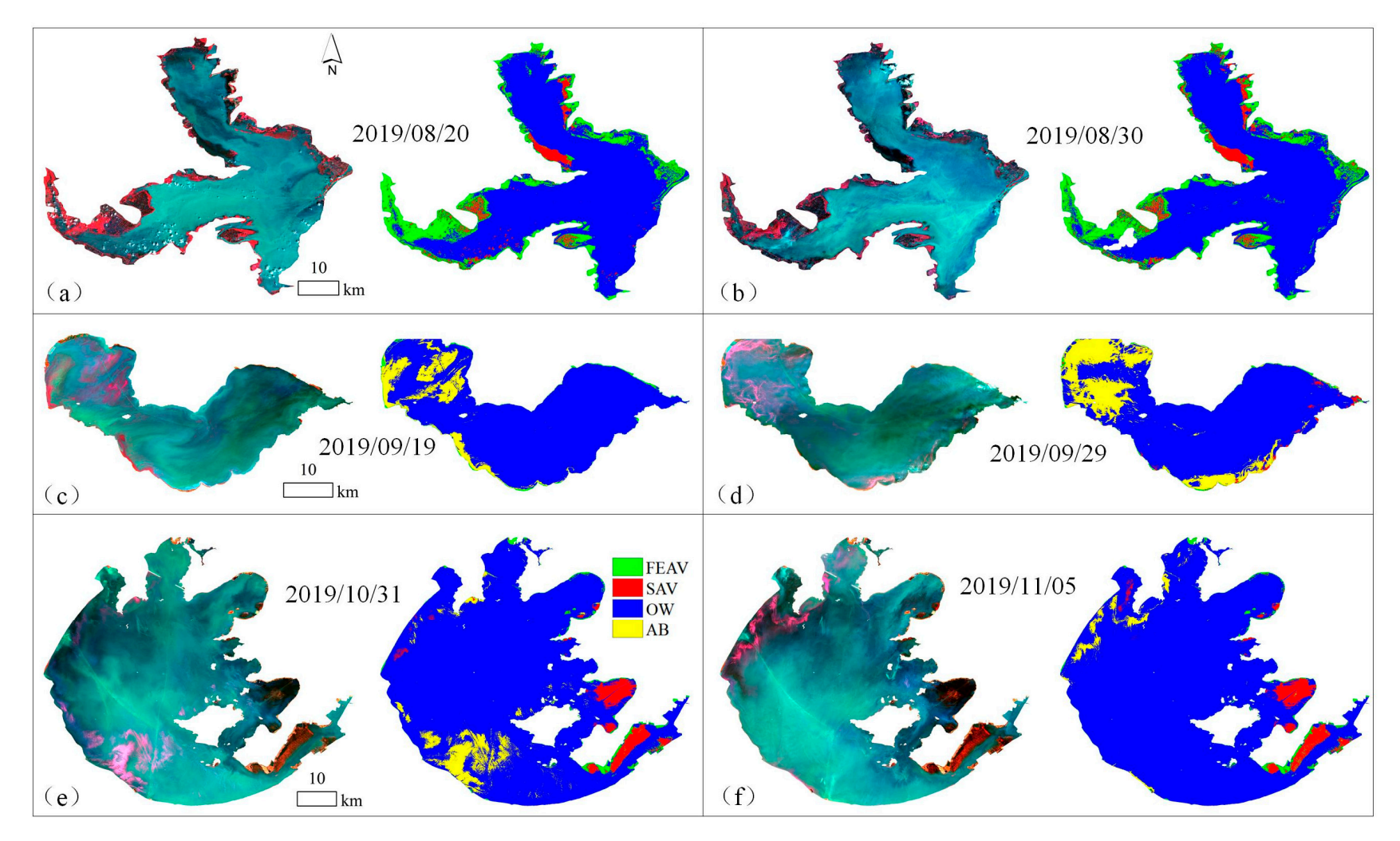


**Figure 5.** False color images (NIR, Red, Green) with neighboring temporal and corresponding classification maps derived from our algorithm in Lake Hongze (**a**,**b**), Lake Chaohu (**c**,**d**) and Lake Taihu (**e**,**f**).

Land 2025, 14, 592 11 of 18

## 4.1.3. Comparison with Published Maps

We also compared the maps obtained in this study and from published studies. Specifically, we selected the classification results of Lake Chaohu and Lake Taihu from published studies [10,13,14], and acquired the maps derived from our algorithm that were closest in time. The results show that, despite slight differences in local areas due to variations in satellite data sources and image acquisition times, the overall classification results are consistent (Figure 6).

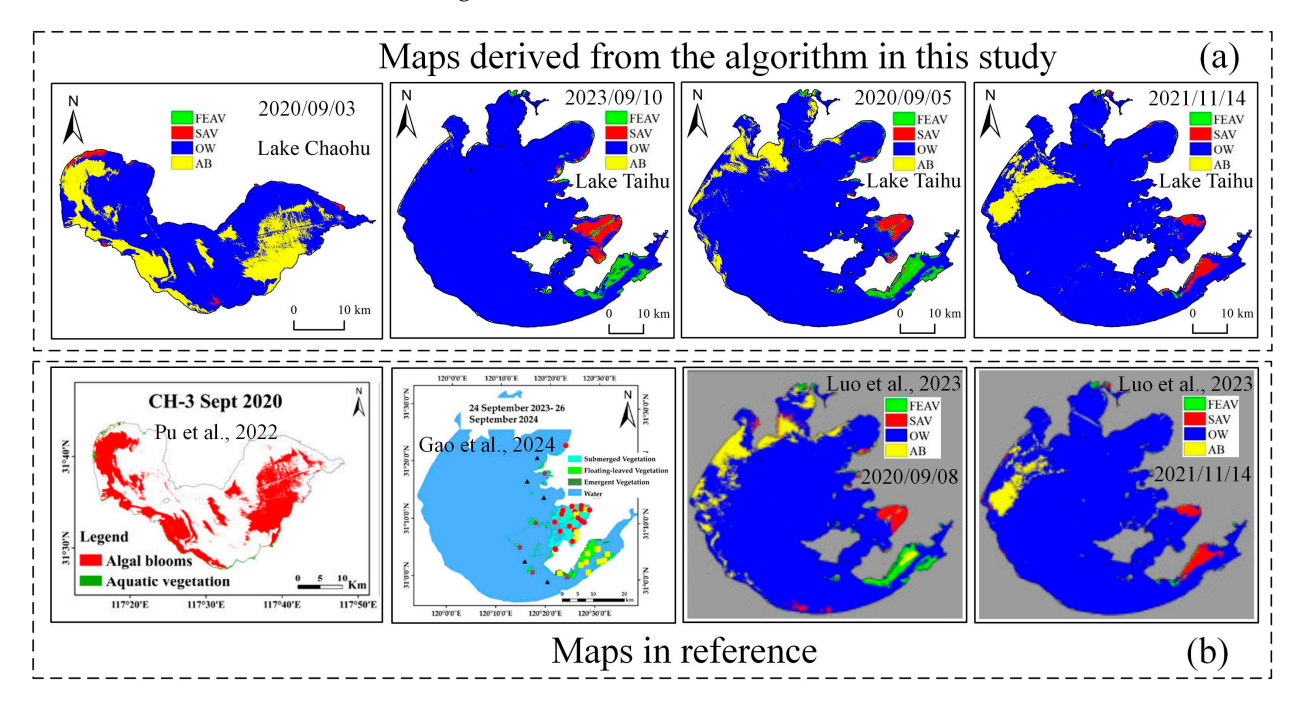


**Figure 6.** Comparison of maps derived from the algorithm in this study (a) and in published studies (b) [10,13,14].

#### 4.2. Algorithm Applications

The algorithm was applied to Sentinel data for obtaining annual and interannual changes of SAV, FEAV and AB from 2019 to 2023 in Lake Hongze, Lake Chaohu, and Lake Taihu (Figures 7 and 8). The results revealed that AB frequently occurs in autumn and has been decreasing over the past five years. Specifically, in Lake Taihu, were primarily distributed in the northern and western parts, and the maximum distribution area of AB has significantly decreased each year from 2019 to 2023 ( $R^2 = 0.06$ , p < 0.05) (Figures 7a and 8c). In 2023, the maximum distribution area of AB decreased by approximately 70% compared to 2019. In Lake Hongze, AB was observed only in 2020 and 2021, with the maximum distribution area decreasing from 59.8 km² to 39.8 km² (Figure 7c). In Lake Chaohu, the maximum distribution area of AB has also continuing decreased from 435.9 km² to 165.7 km², and this trend is significant from 2019 to 2023 ( $R^2 = 0.15$ , p < 0.01) (Figures 7e and 8b).

In addition, the results also revealed that the phenological characteristics of aquatic vegetation within the year and changes over the past five years. Specifically, the distribution area of aquatic vegetation in Lake Hongze and Lake Taihu is largest during the summer and autumn (Figure 8a,c). From 2019 to 2023, aquatic vegetation exhibited a decreasing trend in both two lakes, with the area in Lake Taihu decreasing from 304.4 km² to 254.9 km², and in Lake Hongze from 598.7 km² to 399.2 km², respectively (Figure 7b,d). The long-term changes also indicate that Lake Taihu is a lake dominated by SAV, while Lake Hongze is dominated by FEAV. In contrast, the extent of aquatic vegetation in Lake Chaohu is significantly smaller than that in the other two lakes, remaining at around

10 km<sup>2</sup> (Figure 7f). This may be attributed to the fact that Lake Chaohu only has emergent vegetation distributed in the lakeshore zone (Figure 8b).

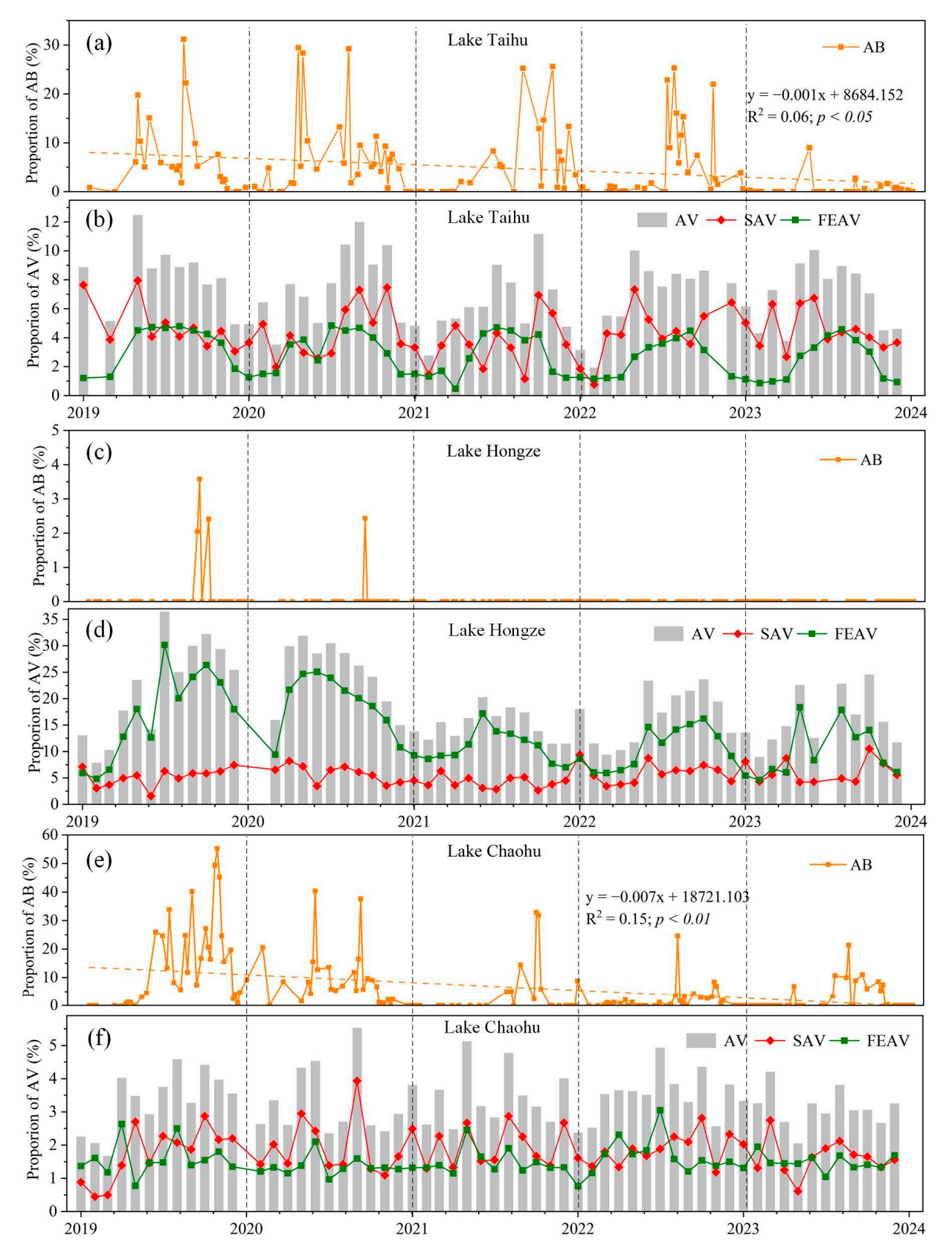


**Figure 7.** Area change of AB, SAV, and FEAV in Lake Taihu (**a**,**b**), Lake Hongze (**c**,**d**), and Lake Chaohu (**e**,**f**) from 2019 to 2023.

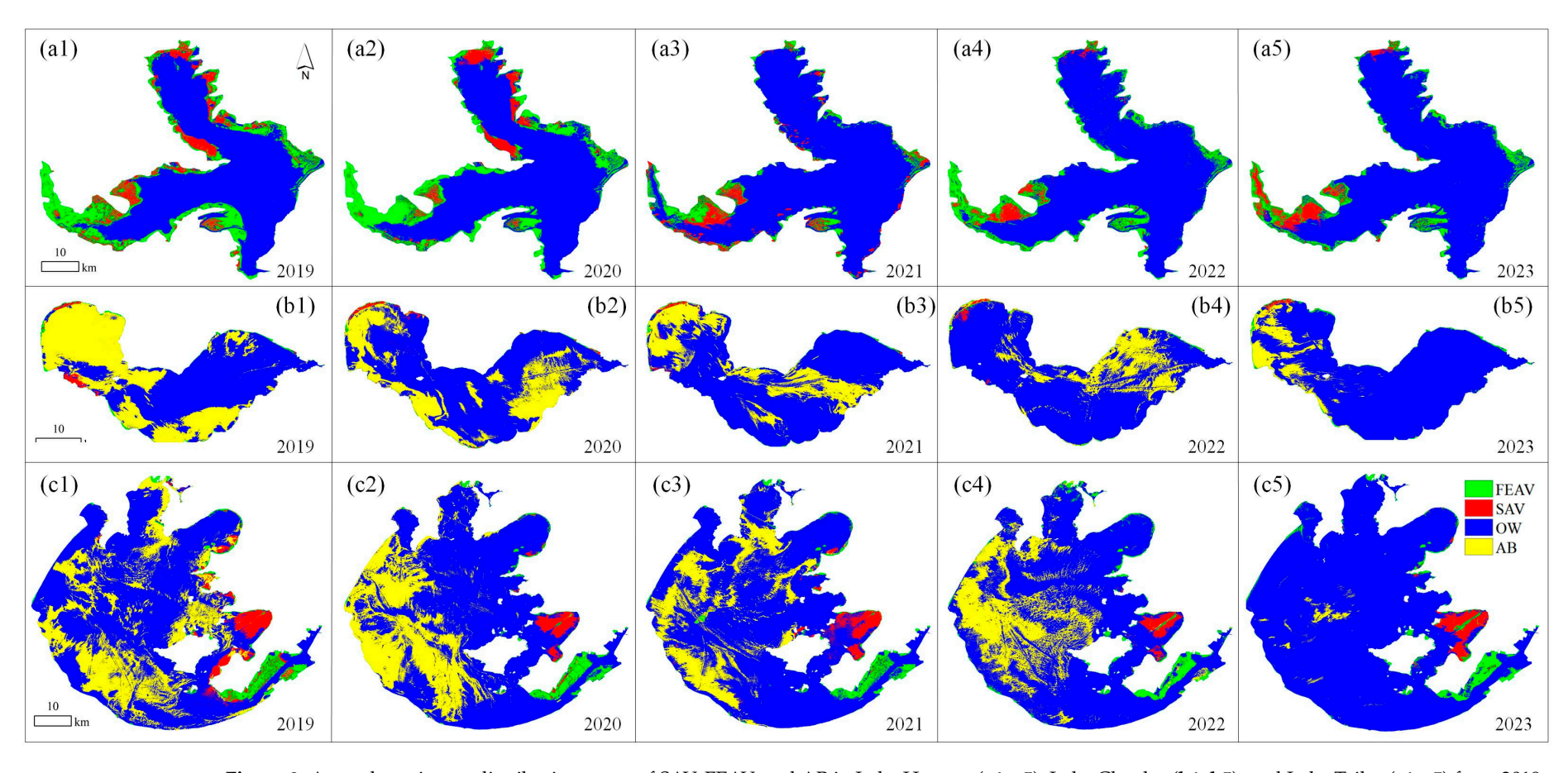


Figure 8. Annual maximum distribution maps of SAV, FEAV, and AB in Lake Hongze (a1-a5), Lake Chaohu (b1-b5), and Lake Taihu (c1-c5) from 2019 to 2023.

Land 2025, 14, 592 14 of 18

# 5. Discussion

## 5.1. Advantages

The algorithm proposed in this study is a comprehensive, automated and robust approach based on Sentinel data, which fully leverages the unique red-edge bands and the high spatial and temporal resolution of Sentinel-2 MSI data. Although the red edge bands of Sentinel-2 MSI have been widely used to identify aquatic vegetation or algal bloom, previous studies often map these features independently, focusing on only one of them [18,39,40]. In fact, aquatic vegetation and algal blooms often coexist in eutrophic lakes, and such independent approaches are not conducive to studying lake regime shifts. Few studies have explored whether red-edge bands can effectively distinguish between these two features, which both exhibit typical vegetation spectral characteristics. In this study, we addressed this issue by providing a band combination method, specifically using the red edge bands (B5-7, B8A) and other bands (B3, B8, and B11, B12) to construct PC2. PC2 is the first index entirely developed based on Sentinel-2 MSI data for separating FEAV and AB, and it forms the core of the algorithm proposed in this study. Notably, removing the red-edge bands from PC2 significantly reduces its ability to distinguish FEAV and AB (Figure S2). In addition, the adaptability of PC2 and SSAVI to complex lake environments endows the monitoring algorithm proposed in this study with high accuracy and robustness. Additionally, the adaptability of PC2 and SSAVI to complex lake environments enhances the accuracy and robustness of the monitoring algorithm. In three typical lakes with distinct water environments and ecological features—Lake Taihu, where aquatic vegetation and AB coexist; Lake Hongze, dominated by FEAV; and Lake Chaohu, characterized by sparse aquatic vegetation and persistent AB—the algorithm achieved an average overall classification accuracy of 92.66% (Table 2). In the long-term monitoring of aquatic vegetation and AB in these three lakes, the algorithm exhibited high stability, with phenological changes aligning with observed data [33,41]. Overall, the proposed algorithm shows significant potential for large-scale spatiotemporal monitoring of FEAV and AB dynamics in lakes.

#### 5.2. Limitations

The SSAVI-GMM algorithm for mapping SAV in this study lies in the fusion of Sentinel-2 MSI and Sentinel-1 SAR data. Due to the inconsistent temporal resolution of MSI and SAR data, the time interval between the Sentinel-2 MSI and Sentinel-1 SAR images used for fusion directly affects the SSAVI index. Theoretically, a shorter time interval between the two data sources results in better classification outcomes. However, a shorter interval also means fewer images can be used for fusion. The time interval of the fused images significantly influences the classification results, as mismatched image fusion can lead to a decline in image quality. Therefore, this study selected SAR images for fusion that were acquired within 10 days before and after the optical images [12]. Additionally, the reduced quality of fused images caused by the time gap between optical and SAR imagery may also affect the parameters of the X-means clustering algorithm. The range of the cluster number parameter needs to be expanded to meet mapping requirements.

PC2, used for separating FEAV and AB, requires eight bands of Sentinel-2 MSI image: B3, B5-7, B8A, B8, B11, and B12. During our testing of other band combinations from Sentinel-2 MSI, we found that PC2 effectively separates FEAV and AB only when using the eight-band combination employed in this study. In contrast, when only the six bands common to both Sentinel-2 and Landsat were used, including the visible bands (B2-4), near-infrared (B8), and short-wave infrared bands (B11, B12), PC2 was unable to achieve the separation of FEAV and AB [33]. We believe that the red edge bands are critical for the

Land 2025, 14, 592 15 of 18

effectiveness of PC2 in differentiating FEAV and AB. Therefore, this algorithm may not be applicable to satellites lacking red edge bands, such as Landsat and MODIS.

# 5.3. Implications

The algorithm proposed in this study for mapping FEAV, SAV, and AB based on Sentinel-1 SAR and Sentinel-2 MSI data can continuously and accurately capture the changes of aquatic vegetation and AB in eutrophic lakes. This capability is essential for assessing lake state transitions and ecological restoration in large-scale lakes [4]. In the future, with ongoing improvements and expansions in algorithm applicability, we will reconstruct high spatiotemporal resolution data of FEAV, SAV, and AB in global shallow lakes using the big data platform GEE. This will provide critical data support for understanding the ecological mechanisms and ecosystem services of aquatic vegetation and AB at macro scales [42,43].

Aquatic vegetation, as the primary producer in lake ecosystems, has a significant capacity to absorb and store large amounts of carbon dioxide [44,45]. For example, SAV can directly influence air-water exchange by assimilating large quantities of dissolved inorganic carbon through photosynthesis during the daytime, effectively reducing water column pCO<sub>2</sub> [46]. Some studies also indicated that omitting carbon sequestration by aquatic vegetation in lake ecosystems could lead to an overestimation of the net ecosystem exchange of  $CO_2$  by up to fivefold [47]. However, the role of aquatic vegetation is often underrepresented in current research on lake carbon sources and sinks [48,49]. This introduces substantial uncertainty in research of  $CO_2$  sources, sinks and fluxes in lakes. The fundamental reason for this uncertainty lies in the lack of high spatial-temporal resolution and precision aquatic vegetation and AB data. The algorithm proposed in this study will help fill this gap in estimating carbon fluxes at lake or regional scales.

#### 6. Conclusions

In this study, we developed an automatic algorithm using Sentinel-1 SAR and Sentinel-2 MSI data for mapping SAV, FEAV, and AB in Lake Taihu with the coexistence of aquatic vegetation and AB. We tested the algorithm in three lakes with significantly different water environments, achieving an overall classification accuracy of 87.65%. We also evaluated the algorithm based on the phenological changes of aquatic vegetation, and the algorithm demonstrated robustness. Based on the algorithm, we obtained the annual and interannual variations of AB and FEAV in Lake Taihu, Lake Hongze, and Lake Chaohu. The results indicate that the AB in all three lakes showed a significant decrease from 2019 to 2023. The aquatic vegetation in Lake Taihu and Lake Hongze showed a declining trend, while the aquatic vegetation in Lake Chaohu was spare and remained relatively stable. This algorithm has potential applications for monitoring the spatiotemporal changes of aquatic vegetation and algal blooms in large-scale lakes, providing technical support for future lake ecological assessments and carbon source-sink accounting.

**Supplementary Materials:** The following supporting information can be downloaded at: https://www.mdpi.com/article/10.3390/land14030592/s1.

**Author Contributions:** Conceptualization, Y.X. (Yihao Xin), J.L., J.Z., K.W. and C.C.; Methodology, Y.X. (Yihao Xin), J.L. and K.W.; Validation, J.Z.; Formal analysis, J.Z.; Resources, K.W.; Data curation, Y.X. (Yihao Xin) and Y.X. (Ying Xu); Writing—original draft, Y.X. (Yihao Xin) and J.Z.; Writing—review & editing, Y.X. (Yihao Xin), J.L., Y.X. (Ying Xu) and H.Q.; Visualization, J.Z. and H.Q.; Supervision, J.L.; Project administration, J.L., B.Y. and Q.C.; Funding acquisition, J.L. and B.Y. All authors have read and agreed to the published version of the manuscript.

**Funding:** The study was supported jointly by Open Fund of the National Environmental Protection Key Laboratory of Water Ecological Health in the Middle and Lower Reaches of the Yangtze River (AEHKF2023001). We also thank several anonymous reviewers for their help in improving our manuscript.

**Data Availability Statement:** The data presented in this study are available on request from the corresponding author. The data are not publicly available due to privacy.

Conflicts of Interest: The authors declare no conflict of interest.

## References

- 1. Kosten, S.; Piñeiro, M.; de Goede, E.; de Klein, J.; Lamers, L.P.M.; Ettwig, K. Fate of Methane in Aquatic Systems Dominated by Free-Floating Plants. *Water Res.* **2016**, *104*, 200–207. [CrossRef]
- 2. Zeng, Q.; Wei, Z.; Yi, C.; He, Y.; Luo, M. The Effect of Different Coverage of Aquatic Plants on the Phytoplankton and Zooplankton Community Structures: A Study Based on a Shallow Macrophytic Lake. *Aquat. Ecol.* **2022**, *56*, 1347–1358. [CrossRef]
- 3. Zhang, X. Effects of Benthic-Feeding Common Carp and Filter-Feeding Silver Carp on Benthic-Pelagic Coupling: Implications for Shallow Lake Management. *Ecol. Eng.* **2016**, *88*, 256–264. [CrossRef]
- 4. Janssen, A.B.G.; Hilt, S.; Kosten, S.; De Klein, J.J.M.; Paerl, H.W.; Van De Waal, D.B. Shifting States, Shifting Services: Linking Regime Shifts to Changes in Ecosystem Services of Shallow Lakes. *Freshw. Biol.* **2021**, *66*, 1–12. [CrossRef]
- 5. Hou, X.; Feng, L.; Dai, Y.; Hu, C.; Gibson, L.; Tang, J.; Lee, Z.; Wang, Y.; Cai, X.; Liu, J.; et al. Global Mapping Reveals Increase in Lacustrine Algal Blooms over the Past Decade. *Nat. Geosci.* **2022**, *15*, 130–134. [CrossRef]
- 6. Zhang, Y.; Jeppesen, E.; Liu, X.; Qin, B.; Shi, K.; Zhou, Y.; Thomaz, S.M.; Deng, J. Global Loss of Aquatic Vegetation in Lakes. *Earth-Sci. Rev.* **2017**, *173*, 259–265. [CrossRef]
- 7. Liu, D.; Ding, H.; Han, X.; Lang, Y.; Chen, W. Mapping Algal Blooms in Aquatic Ecosystems Using Long-Term Landsat Data: A Case Study of Yuqiao Reservoir from 1984–2022. *Remote Sens.* **2023**, *15*, 4317. [CrossRef]
- 8. Oyama, Y.; Matsushita, B.; Fukushima, T. Distinguishing Surface Cyanobacterial Blooms and Aquatic Macrophytes Using Landsat/TM and ETM + Shortwave Infrared Bands. *Remote Sens. Environ.* **2015**, *157*, *35*–47. [CrossRef]
- 9. Qing, S.; Runa, A.; Shun, B.; Zhao, W.; Bao, Y.; Hao, Y. Distinguishing and Mapping of Aquatic Vegetations and Yellow Algae Bloom with Landsat Satellite Data in a Complex Shallow Lake, China during 1986–2018. *Ecol. Indic.* **2020**, *112*, 106073. [CrossRef]
- 10. Luo, J.; Ni, G.; Zhang, Y.; Wang, K.; Shen, M.; Cao, Z.; Qi, T.; Xiao, Q.; Qiu, Y.; Cai, Y.; et al. A New Technique for Quantifying Algal Bloom, Floating/Emergent and Submerged Vegetation in Eutrophic Shallow Lakes Using Landsat Imagery. *Remote Sens. Environ.* 2023, 287, 113480. [CrossRef]
- 11. Xu, D.; Pu, Y.; Zhu, M.; Luan, Z.; Shi, K. Automatic Detection of Algal Blooms Using Sentinel-2 MSI and Landsat OLI Images. *IEEE J. Sel. Top. Appl. Earth Obs. Remote Sens.* **2021**, *14*, 8497–8511. [CrossRef]
- 12. Xin, Y.; Luo, J.; Xu, Y.; Sun, Z.; Qi, T.; Shen, M.; Qiu, Y.; Xiao, Q.; Huang, L.; Zhao, J.; et al. SSAVI-GMM: An Automatic Algorithm for Mapping Submerged Aquatic Vegetation in Shallow Lakes Using Sentinel-1 SAR and Sentinel-2 MSI Data. *IEEE Trans. Geosci. Remote Sens.* **2024**, *62*, 4416610. [CrossRef]
- 13. Gao, H.; Li, R.; Shen, Q.; Yao, Y.; Shao, Y.; Zhou, Y.; Li, W.; Li, J.; Zhang, Y.; Liu, M. Deep-Learning-Based Automatic Extraction of Aquatic Vegetation from Sentinel-2 Images—A Case Study of Lake Honghu. *Remote Sens.* **2024**, *16*, 867. [CrossRef]
- 14. Pu, J.; Song, K.; Lv, Y.; Liu, G.; Fang, C.; Hou, J.; Wen, Z. Distinguishing Algal Blooms from Aquatic Vegetation in Chinese Lakes Using Sentinel 2 Image. *Remote Sens.* **2022**, *14*, 1988. [CrossRef]
- 15. Rodríguez-Garlito, E.C.; Paz-Gallardo, A.; Plaza, A. Mapping Invasive Aquatic Plants in Sentinel-2 Images Using Convolutional Neural Networks Trained with Spectral Indices. *IEEE J. Sel. Top. Appl. Earth Obs. Remote Sens.* **2023**, *16*, 2889–2899. [CrossRef]
- 16. Yan, K.; Li, J.; Zhao, H.; Wang, C.; Hong, D.; Du, Y.; Mu, Y.; Tian, B.; Xie, Y.; Yin, Z.; et al. Deep Learning-Based Automatic Extraction of Cyanobacterial Blooms from Sentinel-2 MSI Satellite Data. *Remote Sens.* 2022, 14, 4763. [CrossRef]
- Song, B.; Park, K. Detection of Aquatic Plants Using Multispectral UAV Imagery and Vegetation Index. Remote Sens. 2020, 12, 387.
  [CrossRef]
- 18. Kislik, C.; Dronova, I.; Grantham, T.E.; Kelly, M. Mapping Algal Bloom Dynamics in Small Reservoirs Using Sentinel-2 Imagery in Google Earth Engine. *Ecol. Indic.* **2022**, *140*, 109041. [CrossRef]
- 19. Luo, J.; Ma, R.; Duan, H.; Hu, W.; Zhu, J.; Huang, W.; Lin, C. A New Method for Modifying Thresholds in the Classification of Tree Models for Mapping Aquatic Vegetation in Taihu Lake with Satellite Images. *Remote Sens.* **2014**, *6*, 7442–7462. [CrossRef]
- 20. Ying, A.; Yonghong, B.; Zhengyu, H. Response of Predominant Phytoplankton Species to Anthropogenic Impacts in Lake Taihu. *J. Freshw. Ecol.* **2015**, *30*, 99–112. [CrossRef]
- 21. Wang, H.; Zhang, X.; Peng, Y.; Wang, H.; Wang, X.; Song, J.; Fei, G. Restoration of Aquatic Macrophytes with the Seed Bank Is Difficult in Lakes with Reservoir-like Water-Level Fluctuations: A Case Study of Chaohu Lake in China. *Sci. Total Environ.* **2022**, 813, 151860. [CrossRef]

Land 2025, 14, 592 17 of 18

22. Gargiulo, M.; Dell'Aglio, D.A.G.; Iodice, A.; Riccio, D.; Ruello, G. Integration of Sentinel-1 and Sentinel-2 Data for Land Cover Mapping Using W-Net. *Sensors* **2020**, *20*, 2969. [CrossRef]

- 23. Rao, P.; Zhou, W.; Bhattarai, N.; Srivastava, A.K.; Singh, B.; Poonia, S.; Lobell, D.B.; Jain, M. Using Sentinel-1, Sentinel-2, and Planet Imagery to Map Crop Type of Smallholder Farms. *Remote Sens.* **2021**, *13*, 1870. [CrossRef]
- 24. Lee, J.-S.; Wen, J.-H.; Ainsworth, T.L.; Chen, K.-S.; Chen, A.J. Improved Sigma Filter for Speckle Filtering of SAR Imagery. *IEEE Trans. Geosci. Remote Sens.* **2009**, *47*, 202–213. [CrossRef]
- 25. Messager, M.L.; Lehner, B.; Grill, G.; Nedeva, I.; Schmitt, O. Estimating the Volume and Age of Water Stored in Global Lakes Using a Geo-Statistical Approach. *Nat. Commun.* **2016**, *7*, 13603. [CrossRef] [PubMed]
- Pohl, C.; Van Genderen, J.L. Review Article Multisensor Image Fusion in Remote Sensing: Concepts, Methods and Applications. Int. J. Remote Sens. 1998, 19, 823–854. [CrossRef]
- 27. Wang, Z.; Ziou, D.; Armenakis, C.; Li, D.; Li, Q. A Comparative Analysis of Image Fusion Methods. *IEEE Trans. Geosci. Remote Sens.* **2005**, *43*, 1391–1402. [CrossRef]
- 28. Kim, Y.; Van Zyl, J. Comparison of Forest Parameter Estimation Techniques Using SAR Data. In Proceedings of the IGARSS 2001, Scanning the Present and Resolving the Future. Proceedings, IEEE 2001 International Geoscience and Remote Sensing Symposium (Cat. No.01CH37217), Sydney, NSW, Australia, 9–13 July 2001; Volume 3, pp. 1395–1397.
- 29. Pelleg, D.; Moore, A. X-Means: Extending K-Means with E Cient Estimation of the Number of Clusters. In Proceedings of the Seventeenth International Conference on Machine Learning (ICML 2000), Standord, CA, USA, 29 June–2 July 2000; pp. 727–734.
- 30. Abdi, H.; Williams, L.J. Principal Component Analysis. Wiley Interdiscip. Rev. Comput. Stat. 2010, 2, 433–459. [CrossRef]
- 31. Ghoussein, Y.; Faour, G.; Fadel, A.; Haury, J.; Abou-Hamdan, H.; Nicolas, H. Hyperspectral Discrimination of Eichhornia Crassipes Covers, in the Red Edge and near Infrared in a Mediterranean River. *Biol. Invasions* **2023**, 25, 3619–3635. [CrossRef]
- 32. Jie, L.; Wang, J. Research on the Extraction Method of Coastal Wetlands Based on Sentinel-2 Data. *Mar. Environ. Res.* **2024**, *198*, 106429. [CrossRef]
- 33. Luo, J.; Li, X.; Ma, R.; Li, F.; Duan, H.; Hu, W.; Qin, B.; Huang, W. Applying Remote Sensing Techniques to Monitoring Seasonal and Interannual Changes of Aquatic Vegetation in Taihu Lake, China. *Ecol. Indic.* **2016**, *60*, 503–513. [CrossRef]
- 34. Liang, S.; Gong, Z.; Wang, Y.; Zhao, J.; Zhao, W. Accurate Monitoring of Submerged Aquatic Vegetation in a Macrophytic Lake Using Time-Series Sentinel-2 Images. *Remote Sens.* **2022**, *14*, 640. [CrossRef]
- 35. Ostu, N. A Threshold Selection Method from Gray-Level Histograms. IEEE Trans. SMC 1979, 9, 62.
- 36. Congalton, R.G. A Review of Assessing the Accuracy of Classifications of Remotely Sensed Data. *Remote Sens. Environ.* **1991**, 37, 35–46. [CrossRef]
- 37. Luo, J.; Duan, H.; Ma, R.; Jin, X.; Li, F.; Hu, W.; Shi, K.; Huang, W. Mapping Species of Submerged Aquatic Vegetation with Multi-Seasonal Satellite Images and Considering Life History Information. *Int. J. Appl. Earth Obs. Geoinf.* **2017**, *57*, 154–165. [CrossRef]
- 38. Congalton, R.G. Assessing Landsat Classification Accuracy Using Discrete Multivariate Analysis Statistical Techniques. *Photogramm. Eng.* **1983**, 49, 1671–1678.
- 39. Jia, M.; Wang, Z.; Wang, C.; Mao, D.; Zhang, Y. A New Vegetation Index to Detect Periodically Submerged Mangrove Forest Using Single-Tide Sentinel-2 Imagery. *Remote Sens.* **2019**, *11*, 2043. [CrossRef]
- 40. Thamaga, K.H.; Dube, T. Understanding Seasonal Dynamics of Invasive Water Hyacinth (*Eichhornia crassipes*) in the Greater Letaba River System Using Sentinel-2 Satellite Data. *GIScience Remote Sens.* **2019**, *56*, 1355–1377. [CrossRef]
- 41. Hou, X.; Feng, L.; Chen, X.; Zhang, Y. Dynamics of the Wetland Vegetation in Large Lakes of the Yangtze Plain in Response to Both Fertilizer Consumption and Climatic Changes. *ISPRS J. Photogramm. Remote Sens.* **2018**, *141*, 148–160. [CrossRef]
- 42. Alahuhta, J.; Lindholm, M.; Baastrup-Spohr, L.; García-Girón, J.; Toivanen, M.; Heino, J.; Murphy, K. Macroecology of Macrophytes in the Freshwater Realm: Patterns, Mechanisms and Implications. *Aquat. Bot.* **2021**, *168*, 103325. [CrossRef]
- 43. Thomaz, S.M. Ecosystem Services Provided by Freshwater Macrophytes. Hydrobiologia 2023, 850, 2757–2777. [CrossRef]
- 44. Regnier, P.; Resplandy, L.; Najjar, R.G.; Ciais, P. The Land-to-Ocean Loops of the Global Carbon Cycle. *Nature* **2022**, *603*, 401–410. [CrossRef] [PubMed]
- 45. Roth, F.; Broman, E.; Sun, X.; Bonaglia, S.; Nascimento, F.; Prytherch, J.; Brüchert, V.; Lundevall Zara, M.; Brunberg, M.; Geibel, M.C.; et al. Methane Emissions Offset Atmospheric Carbon Dioxide Uptake in Coastal Macroalgae, Mixed Vegetation and Sediment Ecosystems. *Nat. Commun.* 2023, 14, 42. [CrossRef]
- 46. Shen, C.; Qian, M.; Song, Y.; Chen, B.; Yang, J. Surface pCO<sub>2</sub> and Air-Water CO<sub>2</sub> Fluxes Dominated by Submerged Aquatic Vegetation: Implications for Carbon Flux in Shallow Lakes. *J. Environ. Manag.* **2024**, *370*, 122839. [CrossRef] [PubMed]
- 47. Peixoto, R.B.; Marotta, H.; Bastviken, D.; Enrich-Prast, A. Floating Aquatic Macrophytes Can Substantially Offset Open Water CO<sub>2</sub> Emissions from Tropical Floodplain Lake Ecosystems. *Ecosystems* **2016**, *19*, 724–736. [CrossRef]

48. Qi, T.; Xiao, Q.; Cao, Z.; Shen, M.; Ma, J.; Liu, D.; Duan, H. Satellite Estimation of Dissolved Carbon Dioxide Concentrations in China's Lake Taihu. *Environ. Sci. Technol.* **2020**, *54*, 13709–13718. [CrossRef]

49. Ran, L.; Butman, D.E.; Battin, T.J.; Yang, X.; Tian, M.; Duvert, C.; Hartmann, J.; Geeraert, N.; Liu, S. Substantial Decrease in CO<sub>2</sub> Emissions from Chinese Inland Waters Due to Global Change. *Nat. Commun.* **2021**, *12*, 1730. [CrossRef]

**Disclaimer/Publisher's Note:** The statements, opinions and data contained in all publications are solely those of the individual author(s) and contributor(s) and not of MDPI and/or the editor(s). MDPI and/or the editor(s) disclaim responsibility for any injury to people or property resulting from any ideas, methods, instructions or products referred to in the content.